Hindawi
Journal of Nanomaterials
Volume 2020, Article ID 4187074, 11 pages
https://doi.org/10.1155/2020/4187074

Research Article

Numerical Simulation of the Cooling of Heated Electronic Blocks in Horizontal Channel by Mixed Convection of Nanofluids

Mustapha Ait Hssain, Rachid Mir, and Youness El Hammami

Laboratory of Mechanics, Processes, Energy and Environment (LMPEE), National School of Applied Sciences, Ibn Zohr University, Agadir, Morocco

Correspondence should be addressed to Mustapha Ait Hssain; ait.hssain90@gmail.com

Received 15 May 2019; Revised 27 November 2019; Accepted 5 February 2020; Published 29 February 2020

Academic Editor: Francesco Marotti de Sciarra

The present work is devoted to the numerical study of steady and laminar mixed convection of nanofluid (water nanoparticles) in a horizontal channel provided with sources of heat at constant temperature, which simulate hot electronic components. The transport equations for continuity, momentum, and energy are solved with finite volume approach using the SIMPLE algorithm. The effective thermal conductivity and the dynamic viscosity of the nanofluid are calculated using, respectively, the Maxwell-Garnett and Brinkman model. The influence of the volume fraction of the nanoparticles $0\% \le \varphi \le 10\%$, Reynolds numbers $5 \le \mathrm{Re} \le 75$, the distance between the blocks $0 \le d/H \le 3$, and the types of nanoparticles added (TiO_2, Al_2O_3, CuO, Ag, Cu, and MgO) were investigated and discussed. It emerges from this simulation that the heat transfer increases with the increase in the volume fraction of the nanoparticles and the Reynolds number and decreases with the augmentation of separation distance between heated sources. Moreover, the study shows that the heat transfer is improved by 20% at a solid volume fraction of 10% of Cu nanoparticles.

1. Introduction

Mixed convection cooling in a channel is very important in many technological applications such as heat exchanger, electronic components, catalytic reactors, solar collectors, high-performance boilers, and power plants. Indeed, the improvement or reduction of heat transfer in these applications is necessary in order to reach valuable inferences about energy savings. Several research studies on heat transfer have been conducted in recent decades to develop new techniques to improve heat transfer by using metallic or nonmetallic additives in base fluids to enhance their thermal conductivity. Numerous studies, both numerical and experimental, have been conducted on heat transfer by convection with or without the use of nanofluids in different geometries.

Hamouche and Bessaïh [1] numerically studied laminar mixed convection heat transfer of an air flow during the cooling of two identical heat sources simulating electronic components in a horizontal channel. The finite volume approach and the SIMPLER algorithm are used to solve conservation equations for mixed convection. The results obtained reveal that increasing the separation distance, the height, and the width of the components considerably improves the heat removal rate of the components. Mohebbi et al. [2] conducted a Boltzmann method numerical study on forced convection in a large surface channel using different nanofluids. The results show that the average number of Nusselt increases when the volume fraction of nanoparticles increases from 0% to 5%. In addition, the effect of nanoparticles on heat transfer is more noticeable when Reynolds number values are higher. Heidary and Kermani [3] performed a numerical study to heat transfer within a channel with blocks attached to bottom wall and using nanofluid. The differential equations are solved by the finite volume approach and the SIMPLE algorithm. Their results show that heat transfer in the channels is improved by 60% due to the presence of nanoparticles and the blocks. The average Nusselt number does not increase anymore beyond a certain

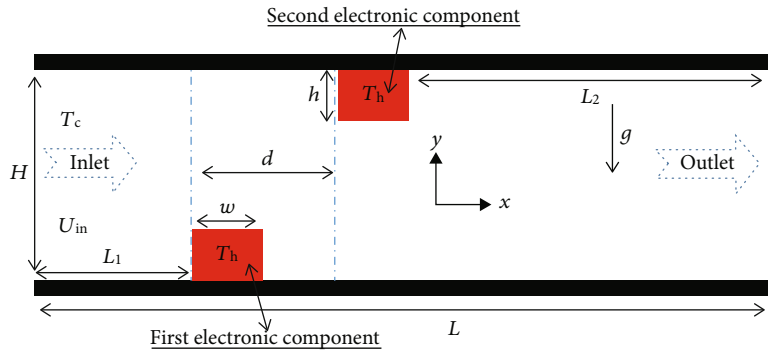

Figure 1: Schematic of the physical model study.

number of blocks. Esfe et al. [4] studied the laminar mixed convection of nanofluid in a horizontal channel provided with two sources of heat at constant temperature mounted on the bottom wall. Their study showed that the rate of heat removal increases as the volume fraction of nanoparticles increases. The average Nusselt number decreases with an increase in obstacle size. Akbarinia and Behzadmehr [5] numerically examined mixed convection of nanofluid in a horizontal tube using three-dimensional elliptic equations. They showed that the volume fraction of added nanoparticles has no direct effect on secondary flow and on the coefficient of friction. The heat transfer by convection of nanofluids due to buoyancy forces in a partially heated rectangular cavity was considered by Oztop et al. [6]. They noticed that the average number of Nusselt increases as the volume fraction of nanoparticles increases and that the heating location affects the fields of flow and temperature when using nanofluids. They also obtained that the improvement of heat transfer, using nanofluids, is more pronounced at low ratio than at high ratio. Huo and Rao [7] numerically studied the cooling enhancement of a battery thermal management (BTM) system utilizing (water-Al_2O_3) nanofluid using the lattice Boltzmann method. Their results show that the addition of nanoparticles reduces the average battery temperature. The average battery temperature was reduced by 7% with an Al_2O_3 volume fraction of 4%. Ambreen et al. [8] conducted a comparative study of numerical models for laminar forced convection of nanofluids in micro- and minichannels. These authors used homogeneous, discrete phase and Eulerian-Eulerian CFD models. The results show that single-phase and two-phase numerical models provide reasonably accurate hydrothermal results for nanofluids with low thermal conductivity. However, the Eulerian-Eulerian models overestimate the thermal transfer coefficient due to the overestimation of volume average thermal conductivity. Sheikholeslami et al. [9] presented a study on forced convection of CuO-water nanofluid in the presence of Lorentz forces using the LBM method. They observed that the increase of Reynolds number and Darcy number leads to an increase in the temperature gradient near the top wall. They also found that the Nusselt number enhances with rise of Hartmann number. Khan et al. [10] presented an analytical study of heat transfer between the nanofluid and the vertical wall using two types of nanoparticles, copper (Cu) and silver (Ag), suspended in water. They used the Laplace transformation method to find the analytic solutions for the velocity and temperature fields. Their results show that heat transfer decreases with an increasing volume fraction of nanoparticles. They also observed that the Hartman number and porosity have opposite effects on fluid motion.

The encouraging results presented in all of the mentioned researches show that the use of the nanofluid improves heat transfer performance in cooling electronic systems. The main objective of this work is to examine mixed convection of the nanofluid in a horizontal channel with two heat sources. A numerical study is carried out to predict the effect of Reynolds number, type of nanoparticles, volume fraction, and block separation distance on the heat transfer rate.

2. Mathematical Model

2.1. Problem Statement. The geometry considered in this study is a two-dimensional horizontal channel with two heat sources, which simulate hot electronic components, one located on the bottom wall of the horizontal channel and the other on the top wall, as shown in Figure 1. The two walls of the channel studied are supposed adiabatic. At the entrance of the channel, a flow velocity U_{in} is imposed with a constant temperature T_C (the cooling water). The heating components are kept at a uniform temperature T_h (hot temperature). The nanofluid in the channel is considered to be Newtonian, incompressible, and laminar. The nanoparticles are supposed to be in thermal equilibrium with the base fluid. The thermophysical properties of pure water and nanoparticles at the temperature of 25°C are given in Table 1, and the thermophysical properties of the nanofluid are presumed to be constant excluding the variation of density which was approached by the Boussinesq model. The Brinkman model and Maxwell-Garnett model are used, respectively, for calculating the effective viscosity and the effective thermal conductivity. The fluid present in this study is a nanofluid based on containing different types of nanoparticles (TiO_2, Al_2O_3, CuO, Ag, Cu, and MgO).

Table 1: Thermophysical properties of the base fluid and the nanoparticles.

Properties	Water	CuO	Al_2O_3	TiO_2	MgO	Ag	Cu
C_p (J/kg·K)	4179	561	765	686.2	955	235	385
ρ (kg/m^3)	997.1	6450	3970	4250	3560	10500	8933
k (W·m·K)	0.613	20	40	8.9538	45	429	400
$\beta \times 10^5$ (K^{-1})	21	1.8	0.85	0.9	1.13	1.89	1.67
$\mu \times 10^4$ (kg/ms)	8.55	—	—	—	—	—	—

2.2. Governing Equations. By using the following dimensionless parameters:

$$X = \frac{x}{H},$$
$$Y = \frac{y}{H},$$
$$U = \frac{u}{U_{in}},$$
$$V = \frac{v}{U_{in}},$$
$$P = \frac{p}{\rho_{nf} U_{in}^2}$$
$$\mathrm{Re} = \frac{\rho_f U_{in} H}{\mu_f},$$
$$\mathrm{Pr} = \frac{\mu_f C_{pf}}{k_f},$$
$$\mathrm{Gr} = \frac{g\beta_f \Delta T H^3}{v_f^2},$$
$$\theta = \frac{T - T_c}{T_h - T_c}. \quad (1)$$

The mass conservation, momentum, and energy equations for two-dimensional problem and steady-state mixed convection can be written in the dimensionless form as follows:

$$\frac{\partial U}{\partial X} + \frac{\partial V}{\partial Y} = 0, \quad (2)$$

$$U\frac{\partial U}{\partial X} + V\frac{\partial U}{\partial Y} = -\frac{\partial P}{\partial X} + \left(\frac{\rho_f \mu_{nf}}{\rho_{nf} \mu_f \,\mathrm{Re}}\right)\left(\frac{\partial^2 U}{\partial X^2} + \frac{\partial^2 U}{\partial Y^2}\right), \quad (3)$$

$$U\frac{\partial V}{\partial X} + V\frac{\partial V}{\partial Y} = -\frac{\partial P}{\partial Y} + \left(\frac{\rho_f \mu_{nf}}{\rho_{nf} \mu_f \,\mathrm{Re}}\right)\left(\frac{\partial^2 V}{\partial X^2} + \frac{\partial^2 V}{\partial Y^2}\right) + \left(\frac{(\rho\beta)_{nf}\mathrm{Gr}}{\rho_{nf}\beta_f \mathrm{ReRe}}\right)\theta, \quad (4)$$

$$U\frac{\partial \theta}{\partial X} + V\frac{\partial \theta}{\partial Y} = \left(\frac{\alpha_{nf}}{\alpha_f \mathrm{RePr}}\right)\left(\frac{\partial^2 \theta}{\partial X^2} + \frac{\partial^2 \theta}{\partial Y^2}\right). \quad (5)$$

The dimensionless boundary conditions are given as follows:

$$\begin{gathered}
\text{Inlet}: \; X = 0;\; U = 1;\; V = 0;\; \theta = 0;\\
\text{Outlet}: \; X = L;\; \frac{\partial U}{\partial X} = 0;\; V = 0;\; \frac{\partial \theta}{\partial X} = 0;\\
\text{Top wall}: \; Y = H;\; U = 0;\; V = 0;\; \frac{\partial \theta}{\partial Y} = 0;\\
\text{Bottom horizontal wall}: \; Y = 0;\; U = 0;\; V = 0;\; \frac{\partial \theta}{\partial Y} = 0;\\
\text{On the first hot component surfaces at bottom wall}: \; \frac{L_1}{H} \le X \le \frac{L_1 + w}{H};\; 0 \le Y \le \frac{h}{H};\; U = V = 0;\; \theta = 1;\\
\text{On the second hot component surfaces at top wall}: \; \frac{L_1 + d}{H} \le X \le \frac{L_1 + d + w}{H};\; \frac{H - h}{H} \le Y \le 1;\; U = V = 0;\; \theta = 1.
\end{gathered} \quad (6)$$

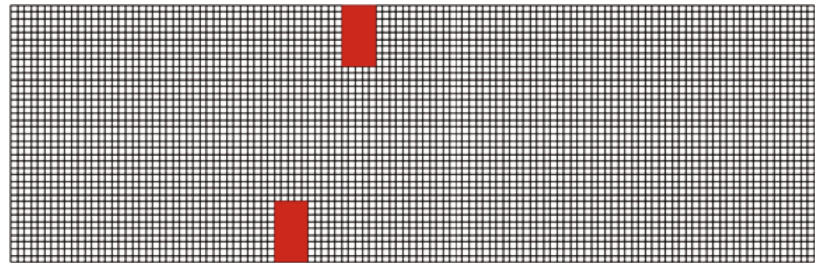

Figure 2: Mesh of the computational domain with grid (41 × 201).

Table 2: Result of the total Nusselt number (Nu_t) for each component for different grids.

Grid size ($y \times x$)	Nu_t(component 1)	Error (%)	Nu_t(component 2)	Error (%)
51 × 501	12.047	3.7	11.4003	1.3
61 × 601	11.5673	0.4	11.3222	2
101 × 601	11.8142	1.7	11.5048	0.45
121 × 701	11.8944	2.4	11.6349	0.67
121 × 1001	11.6142	Ref	11.5571	Ref

2.3. Nanofluid Properties. The nanofluid properties are calculated by the following formulas [11]:

$$\begin{aligned}
\rho_{nf} &= (1-\varphi)\rho_f + \varphi\rho_s,\\
(\rho C_p)_{nf} &= (1-\varphi)(\rho C_p)_f + \varphi(\rho C_p)_s,\\
(\rho\beta)_{nf} &= (1-\varphi)(\rho\beta)_f + \varphi(\rho\beta)_s,\\
\alpha_{nf} &= \frac{k_{nf}}{(\rho C_p)_{nf}}.
\end{aligned} \tag{7}$$

The effective thermal conductivity and the dynamic viscosity of the nanofluid are modeled, respectively, by the Maxwell-Garnett [12] and the Brinkman model [13].

$$\begin{aligned}
\mu_{nf} &= \mu_f(1-\varphi)^{-2.5},\\
k_{nf} &= k_f\left[\frac{k_s + 2k_f - 2\varphi(k_f - k_s)}{k_s + 2k_f + \varphi(k_f - k_s)}\right].
\end{aligned} \tag{8}$$

In order to evaluate the cooling enhancement in the channel, the total Nusselt number and the improvement rates are defined as:

$$\begin{aligned}
Nu_t(\text{component 1}) &= \int_0^{h/H} -\frac{k_{nf}}{k_f}\frac{\partial\theta}{\partial X}\bigg|_{L_1/H} dY + \int_0^{h/H} -\frac{k_{nf}}{k_f}\frac{\partial\theta}{\partial X}\bigg|_{(L_1+w)/H} dY + \int_{L_1/H}^{(L_1+w)/H} -\frac{k_{nf}}{k_f}\frac{\partial\theta}{\partial Y}\bigg|_{h/H} dX,\\
Nu_t(\text{component 2}) &= \int_{(H-h)/H}^{1} -\frac{k_{nf}}{k_f}\frac{\partial\theta}{\partial X}\bigg|_{L_1+d/H} dY + \int_{(H-h)/H}^{1} -\frac{k_{nf}}{k_f}\frac{\partial\theta}{\partial X}\bigg|_{(L_1+d+w)/H} dY + \int_{L_1+d/H}^{(L_1+d+w)/H} -\frac{k_{nf}}{k_f}\frac{\partial\theta}{\partial Y}\bigg|_{(H-h)/H} dX,\\
\varepsilon(\%) &= \frac{Nu_t(\text{nanofluid}) - Nu_t(\text{basefluid})}{Nu_t(\text{basefluid})} \times 100.
\end{aligned} \tag{9}$$

3. Numerical Method and Validation

Governing equations (2)–(5) are solved numerically using the finite volume method [14]. The power scheme is used for the treatment of convection and diffusion terms. The SIMPLE algorithm developed by Patankar [14] is used for the velocity and pressure field coupling. The obtained algebraic equation system is resolved by line-by-line tridiagonal matrix algorithm (TDMA). The total Nusselt number (Nu_t) of the two hot components for five uniform grids (Figure 2) is examined to investigate the independence of the solution from the grid size.

The results for Re = 75, φ = 0%, and Gr = 10^4 are shown in Table 2. As is clear from this table, the uniform grid 101 × 601 is thin enough for the numerical calculation.

The numerical procedure is validated by comparison between the predicted results in the literature with those obtained in this study for mixed convection between two

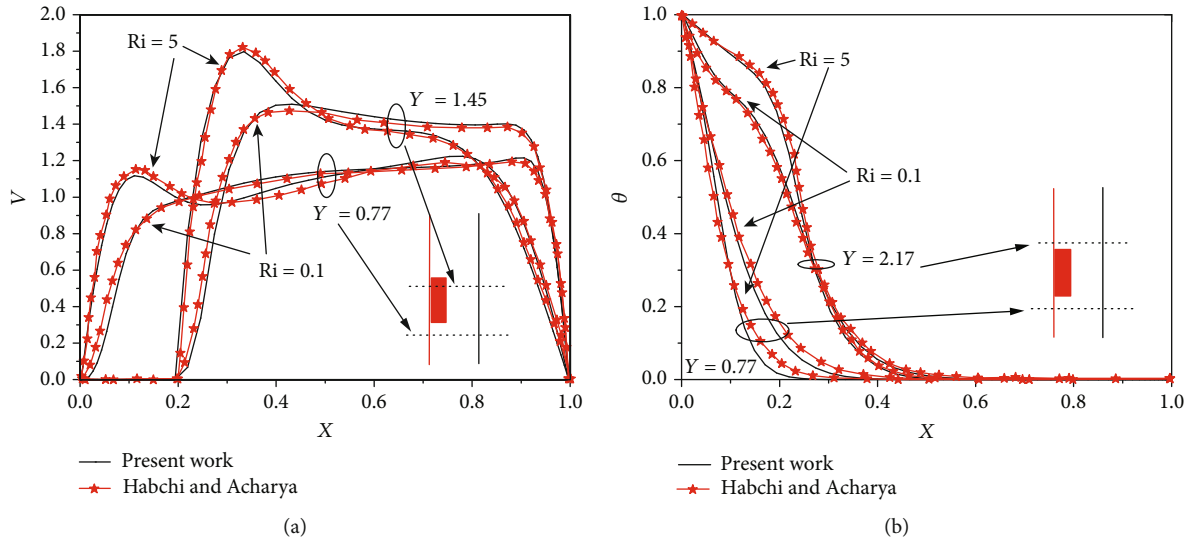

Figure 3: Comparison of (a) velocity and (b) temperature profiles with [15].

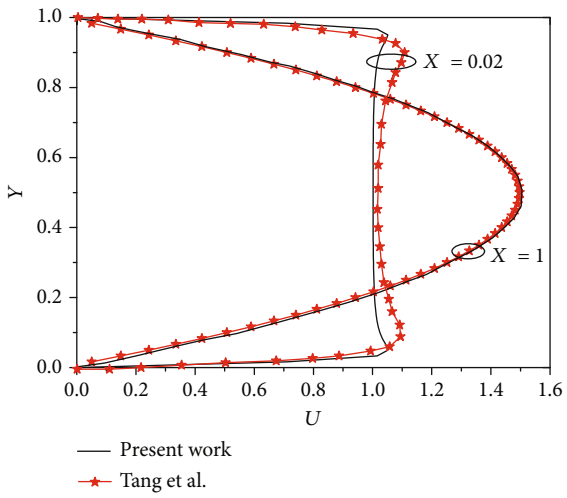

Figure 4: Comparison of velocity profiles with [16].

parallel plates. The first comparison was made with the numerical results found by Habchi and Acharya [15] who treated the case of mixed convection of air as a cooling fluid in a vertical channel. The right wall is adiabatic, and the left wall is at temperature T_h. The component held at a constant temperature is placed in the left wall. Figure 3 shows the comparison between the velocity and temperature profiles found by [15] and that found by the present model. The second comparison with Tang et al. [16] for a Poiseuille flow in a horizontal channel using a uniform inlet velocity $U_{in} = 0.01$. The profiles of dimensionless velocity u/u_{in} at different cross sections $X = 1$ and $X = 0.02$ are shown in Figure 4. From all the figures illustrated, excellent agreement was found between the present calculation and that of Habchi and Acharya [15] and Tang et al. [16]. Then, we can conclude that our code of calculation is valid.

4. Results and Discussions

A numerical study was carried to determine the influence of nanoparticle type, volume fractions, separation distance, and Reynolds number on total Nusselt number of the two components. In this study, the dimensions are taken as follows: $H/H = 1$; $L_1/H = 2$; $w/H = 0.25$; $0 \le d/H \le 3$; $h/H = 0.25$; and $L_2 = L - (L_1 + d + w)$; the distance L_2 must be long enough to ensure the fully developed regime. The details of the configuration of the considered work are illustrated in Figure 1. The Reynolds number varies from 5 to 75. The fraction of the nanoparticles used varies from 0% to 10%.

4.1. Effect of the Type of Nanoparticles with Different Volume Fractions. The effect of types of nanoparticles used on the cooling of electronic components simulated as heat sources was examined by fixing the Reynolds number at $\mathrm{Re} = 75$ and the Grashoff number at $\mathrm{Gr} = 10^4$ for different values of the volume fraction of the nanoparticles ($\varphi = 0\%$, $\varphi = 0.5\%$, $\varphi = 2\%$, $\varphi = 5\%$, and $\varphi = 10\%$). The distance between the components is fixed at $d/H = 2$.

Figures 5 and 6 show the variation in the total Nusselt number for each component for different types of nanoparticles as a function of volume fractions. We observe that the total Nusselt number increases linearly with the increase in the volume fraction of nanoparticles. Two factors influence heat transfer while increasing the volume fraction of nanoparticles: the first is the increase in the viscosity of the nanofluid that slows its movement, which reduces the rate of heat transfer, and the second is the increase in the thermal conductivity of the nanofluid that thus improves conduction heat exchange. The effect of viscosity is less than the effect of conductivity, and therefore, the heat transfer rate increases as the volume fraction of the solid increases. These figures also show the effect of the nanoparticle type on the variation in the total Nusselt number; the heat transfer rate is maximum for copper and silver. A possible explanation for this result is as follows: a high Nusselt number, which means a

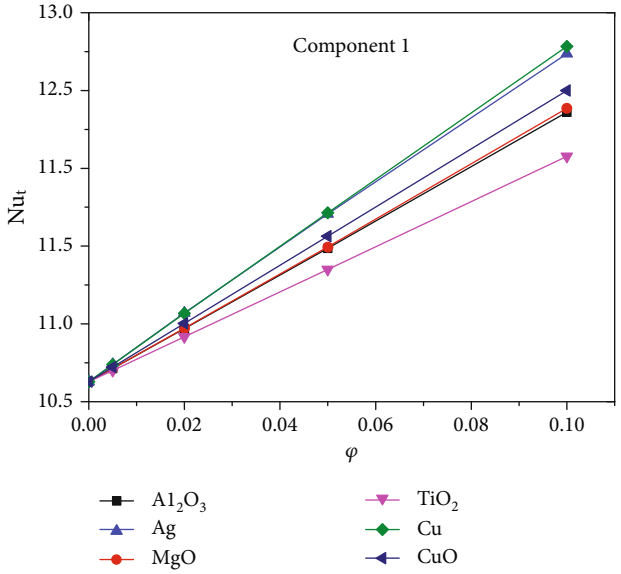

Figure 5: Effects of volume fraction for different nanoparticles on total Nusselt number for the bottom obstacle.

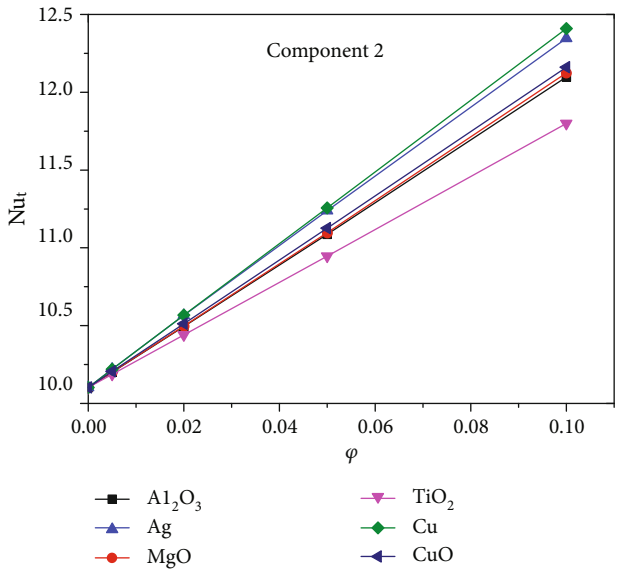

Figure 6: Effects of volume fraction for different nanoparticles on total Nusselt number for the top obstacle.

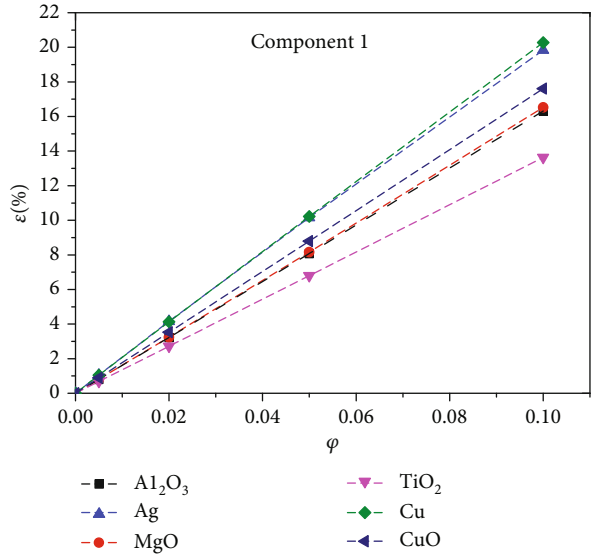

Figure 7: The improvement rate for different nanoparticles versus volume fractions for the bottom obstacle.

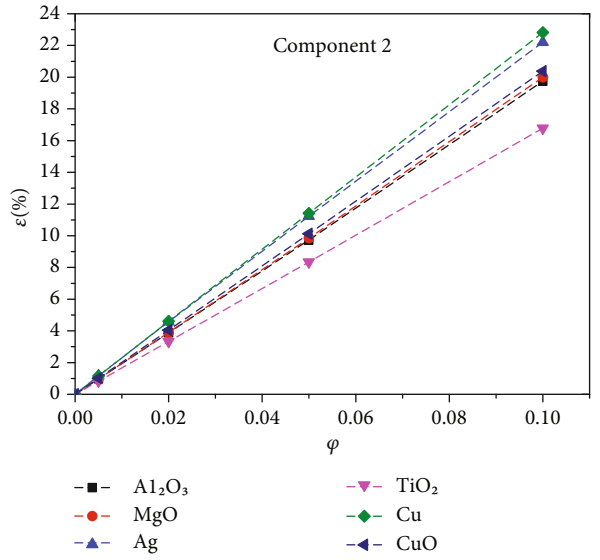

Figure 8: The improvement rate for different nanoparticles versus volume fractions for the top obstacle.

higher exchange, is favored by a higher conductivity to evacuate heat, a lower specific heat to reduce storage, and a higher density to promote convection. These parameters are favorable for copper and silver in comparison to other nanoparticles. For example, Al_2O_3 and TiO_2 nanoparticles have very similar specific heats and densities (difference does not exceed 12%), but the thermal conductivity of Al_2O_3 is about 347% higher than that of TiO_2. Therefore, Al_2O_3 nanoparticles provide better heat transfer than TiO_2 nanoparticles.

To quantitatively evaluate the contribution of different nanoparticles used on heat transfer, we have plotted the heat transfer rate for different volume fractions of the nanoparticles. Figures 7 and 8 clearly show that the rate of improvement increases with the increase in volume fraction of nanoparticles. This improvement is more intense for Cu and Ag nanoparticles, at $\varphi = 10\%$; the improvement is about 20.27% for the bottom component and 22.82% for the top component; also, for TiO_2 nanoparticles, the improvement is 13.63% and 16.78% for the bottom and top components, respectively.

4.2. The Separation Distance Effect. Figure 9 shows the streamlines and isotherms for different separation distances between the two heat sources by setting $Re = 75$ and $Gr = 10^4$ for pure water and water-Cu nanofluid with a volume fraction at $\varphi = 10\%$. The variation of a separation distance between the components ($d/H = 0$, $d/H =$

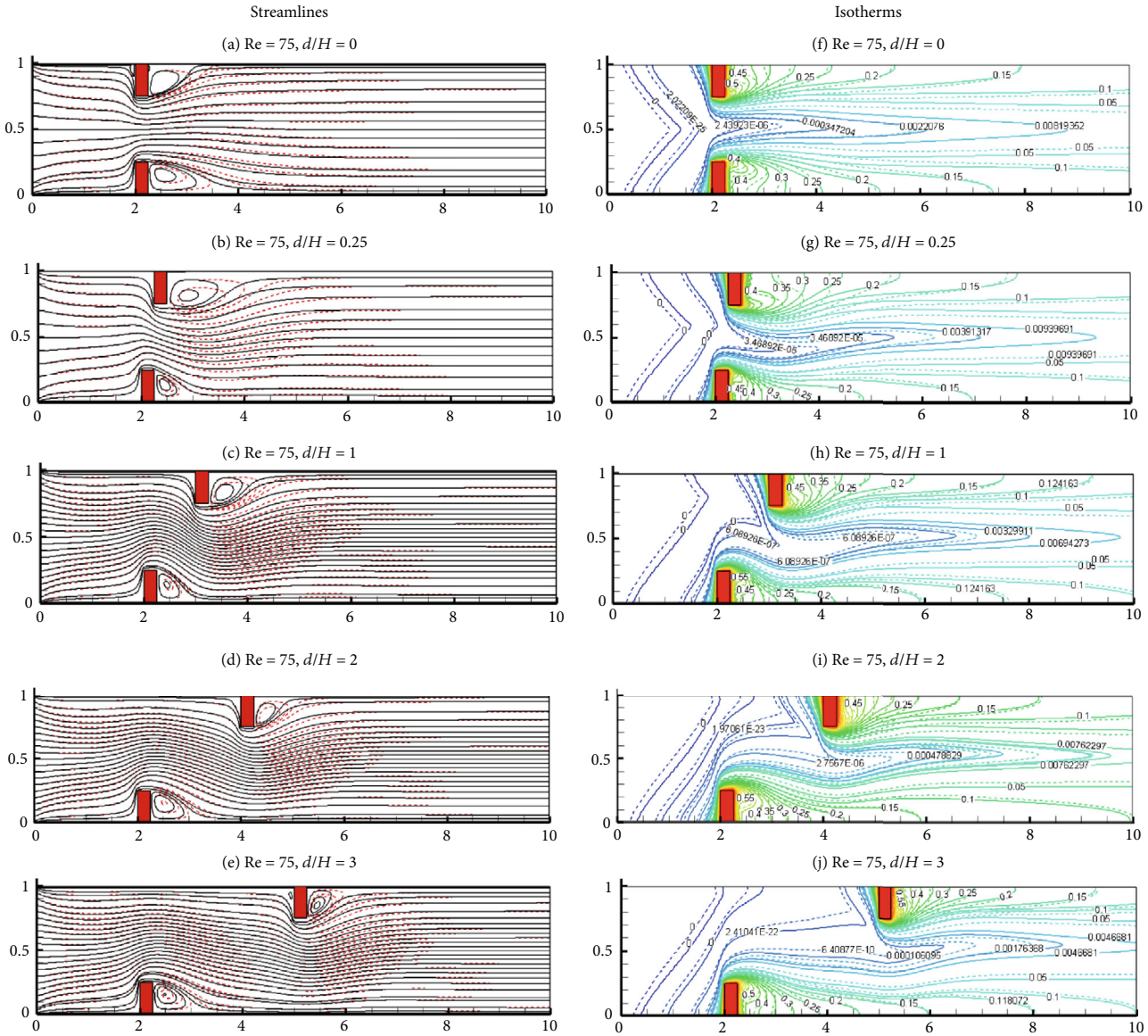

Figure 9: Variations of the streamlines and isotherms versus different separation distances for pure fluid (solid line) and nanofluid (dashed line).

0.25, $d/H = 1$, $d/H = 2$, and $d/H = 3$) makes it possible to evaluate the heat exchange intensity between the cold flow and the hot components in order to find the optimal position of the top component relative to the bottom component. The streamlines plotted in Figures 9(a)–9(e) clearly show recirculation zones behind the blocks in all cases treated, and the flow becomes aligned in the rest of the channel. These recirculation refluxes affect the rate of heat removal from heat sources in these areas. Figures 9(f)–9(j) indicate that the heat transfer thermal boundary layer of the heat source faces decreases as the spacing between the two components increases, and the best transfer is observed when the components are placed symmetrically on the channel walls $d/H = 0$ (Figure 9(f)). This emplacement reduces the cross section of the channel between the two components and therefore increases the flow velocity which reinforces the forced convection allowing a significant heat release and consequently a greater distance of the thermal boundary layer of the components. This evacuation decreases at the level of the upper component as the separation distance increases because the flow already arrives with a quantity of heat extracted from the first component which reduces the heat exchange at the level of the top component.

Figures 10 and 11 show the variation of the total Nusselt number as a function of the separation distance between the two heat sources with different volume fractions of the nanoparticles. These figures show that the heat removal of the bottom component is greater than that of the top component for all the fractions of the nanoparticles used except in the case of the symmetry of the components where we find almost the similar value of the Nusselt. This is due to the fact that both

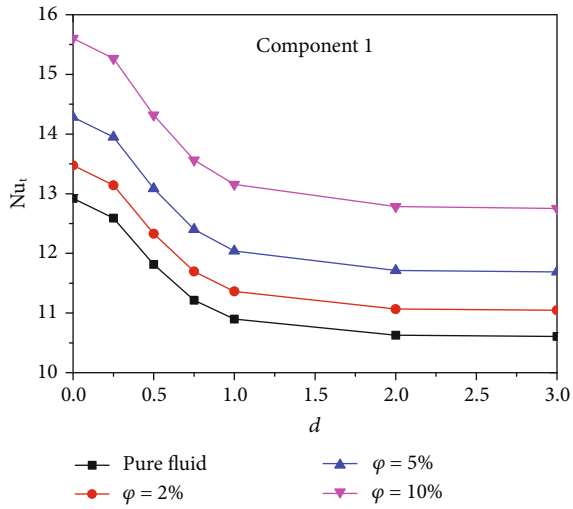

FIGURE 10: Effects of separation distance on the total Nusselt number of the bottom obstacle for different volume fractions.

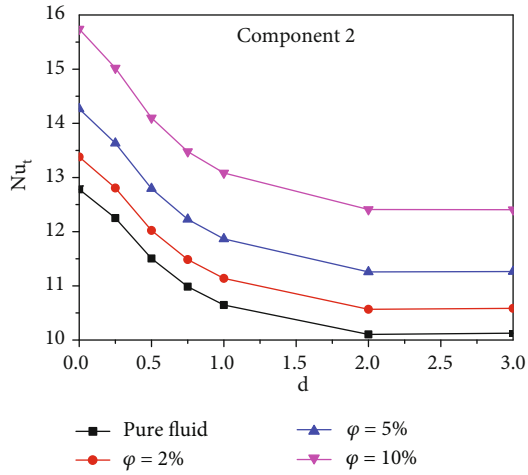

FIGURE 11: Effects of separation distance on the total Nusselt number of the top obstacle for different volume fractions.

components are influenced by flow in the same way; the small variations observed in Nusselt values are due to buoyancy forces. Figures 10 and 11 also show that from a separation distance between the two components greater than $d/H = 2$, the increase in this distance has no significant effect on the heat transfer, and the Nusselt number becomes practically constant. These results confirm that increasing the separation distance is disadvantageous for the heat removal rate for both electronic components. The results show that when the distance between the components increases from $d/H = 0$ to $d/H = 3$, the rate of improvement decreases by about 18% for the lower component and about 21% for the upper component for all fractions of the nanoparticles tested. By increasing the volume fraction of the nanoparticles by 10%, a significant improvement in heat transfer is produced. For the bottom component, the improvement rate is about 21% at $d/H = 0$ and about 20% at $d/H = 3$, and for the top component, the improvement rate is about 23% at $d/H = 0$ and about 22% at $d/H = 3$.

4.3. The Reynolds Number Effect at Different Fractions of Nanoparticles. Figure 12 shows the contours of the streamlines and the isotherms for the pure fluid (solid lines) and for the fluid with nanoparticles with a volume fraction $\varphi = 10\%$ (dashed lines) and by setting $d/H = 2$ and $\mathrm{Gr} = 10^4$. Figures 12(a)–12(d) show the presence of a recirculation zone in front of the top component for $\mathrm{Re} = 5$ because of the buoyancy effects. By augmenting the Reynolds number, this zone disappears. A recirculation zone appears behind the top component as the Reynolds number increases from $\mathrm{Re} = 60$ to $\mathrm{Re} = 75$. This is due to the increase in the obstacle effect when the Reynolds number increases. When the flow approaches the bottom obstacle, it deflects at the upstream corner; a small recirculation zone is formed behind the bottom obstacle. The flow becomes established toward the channel outlet. Figures 12(e)–12(h) illustrate the isotherms for different values of the Reynolds number. It is clear that the temperature field is affected by the variation of the Reynolds number. The isotherms indicated that the thickness of the thermal boundary layer is greater around the upper component since the flow arrives with a heat portion already extracted from the first component for each Reynolds value.

Figure 13 presents the profiles of the velocities in the median plane ($X = 3$) for two values of the Reynolds numbers $\mathrm{Re} = 5$ and $\mathrm{Re} = 75$ for the pure fluid and for the nanofluid. It can be seen that at low Reynolds values ($\mathrm{Re} = 5$), the flow has negative velocities at the left side of the top components and near the top wall, and negative velocities at the bottom of the channel, to the right of the bottom component. This is due to the recirculation zones in these sections (as illustrated in Figure 12(a)). However, we note that the profile of the velocities becomes parabolic as the Reynolds number increases ($\mathrm{Re} = 75$). In Figure 14 which gives the profiles of dimensionless temperature in the median plane ($X = 3$), we observe that for low values of Reynolds number, the temperature near of the bottom component is high; then, it decreases by increasing the Reynolds number. Then, we can say that by increasing the Reynolds number, convection becomes more forced, and this allows for a better heat exchange (see streamlines from Figures 12(a)–12(d)). These findings are valid for both cases without or with the nanoparticles.

Figures 15 and 16 show the effects of the volume fraction of nanoparticles on the total Nusselt number of the two obstacles at different Reynolds numbers ($\mathrm{Re} = 5$, 15, 30, 45, 60, and 75). The addition of nanoparticles will increase the total Nusselt number of both components; in particular, the rate of increase is higher when the nanofluid volume fractions increase. The use of nanoparticles at $\varphi = 10\%$increases the transfer rate by 9.21% for the top component for $\mathrm{Re} = 5$ and 22.82% for $\mathrm{Re} = 75$. For the bottom component, the transfer rate also increases by 12.89% for $\mathrm{Re} = 5$ and by 20.27% for $\mathrm{Re} = 75$. From the comparison of the Nusselt numbers of the two

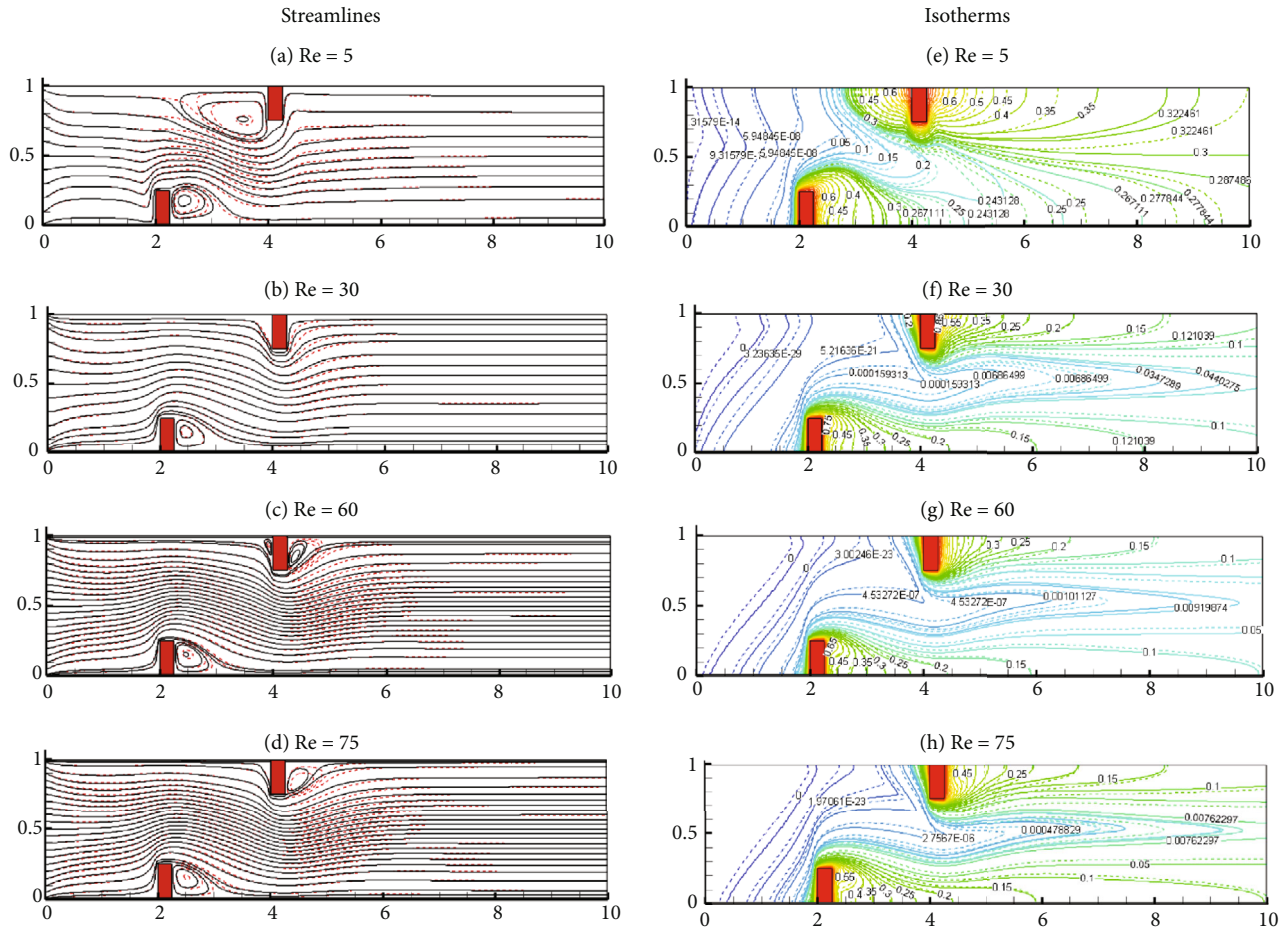

Figure 12: Variations of the streamlines and isotherms versus different Reynolds numbers for pure fluid (solid line) and nanofluid (dashed line).

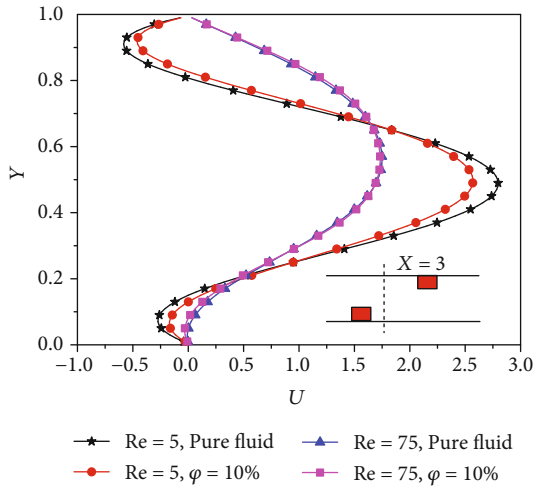

Figure 13: Axial velocity profile for different Reynolds numbers.

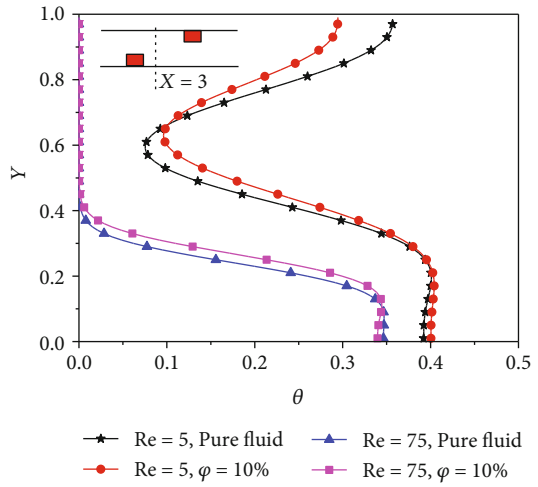

Figure 14: Axial temperature profile for different Reynolds numbers.

components, we found that the bottom component is well cooled compared with that of the top (about 28% for Re = 5 and 3% for Re = 75, for the same volume fraction of nanoparticles $\varphi = 10\%$).

5. Conclusion

A numerical study has been carried out to investigate the laminar mixed convection of nanofluids in an adiabatic

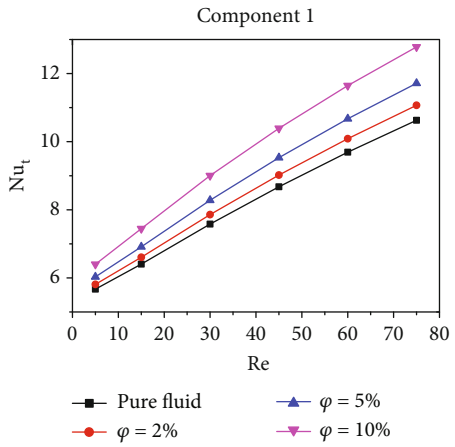

Figure 15: Effects of the Reynolds number on the total Nusselt number of the bottom obstacle for different volume fractions.

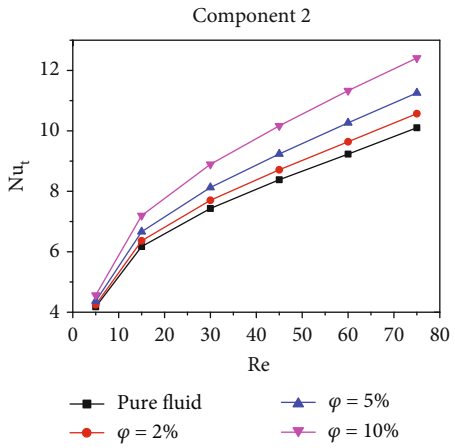

Figure 16: Effects of the Reynolds number on the total Nusselt number of the top obstacle for different volume fractions.

channel with two hot obstacles placed one on the bottom wall and the other on the top wall. The governing equations have been solved using the finite volume method.

The influence of various parameters such as the volume fraction, the Reynolds number, and the separation distance between the components as well as the type of nanoparticles on the heat transfer has been analysed. The main results obtained are listed as follows:

(i) The increase in the volume fraction of the nanofluid improves the cooling of each component

(ii) Increasing the separation distance between the components decreases the heat transfer rate of the electronic components, and the best possible configuration to enhance the cooling of the heated components is that of $d/H = 0$

(iii) It has been found that the improvement of the system cooling is obtained using nanoparticles of copper and silver

(iv) The best system cooling improvement is obtained for Re = 75, $d/H = 0$, $\varphi = 10\%$, Cu, and Ag

(v) As the Reynolds number increases, the total Nusselt number of both components grows and the dimensionless temperature decreases which designate that the heat exchanges become more significant

The results presented in this simulation will be useful for the design of the electronic component cooling system. In the future, the study can be extended for inclined channel, turbulent regimes, and complex geometries.

Nomenclature

C_P: Specific heat ($J \cdot kg^{-1} \cdot K^{-1}$)
d: Distance between sources (m)
Gr: Grashoff number
g: The acceleration of gravity ($m \cdot s^{-2}$)
H: The height of the canal (m)
h: The height of the sources (m)
k: Thermal conductivity ($W \cdot m^{-1} \cdot K^{-1}$)
L: The length of the channel (m)
L_1: The position of the first source (m)
L_2: A distance to ensure the fully developed regime (m)
Nu: Nusselt number
p: Pressure (Pa)
P: Dimensionless pressure
Pr: Prandtl number
Re: Reynolds number
T: Temperature (K)
U, V: Dimensionless velocity components
u, v: Components of velocity ($m \cdot s^{-1}$)
w: The width of the sources (m)
X, Y: Dimensionless Cartesian coordinates
x, y: Cartesian coordinates (m).

Greek Symbols

α: Thermal diffusivity ($m^2 \cdot s^{-1}$)
β: Thermal expansion coefficient of the fluid (K-1)
ε: Improvement rate
θ: Dimensionless temperature
μ: Dynamic viscosity ($kg \cdot m^2 \cdot s^{-1}$)
ν: Kinematic viscosity ($m^2 \cdot s^{-1}$)$[m^2.s^{-1}]$
ρ: Density ($kg \cdot m^{-3}$)
φ: Volume fraction of the nanoparticle.

Subscripts

c: Cold
f: Fluid
h: Hot
in: Inlet
nf: Nanofluid
s: Solid
t: Total.

Data Availability

Data Deposited in a Repository

Conflicts of Interest

The authors declare that they have no conflicts of interest regarding the publication of this paper.

References

[1] A. Hamouche and R. Bessaïh, "Mixed convection air cooling of protruding heat sources mounted in a horizontal channel," *International Communications in Heat and Mass Transfer*, vol. 36, no. 8, pp. 841–849, 2009.

[2] R. Mohebbi, M. M. Rashidi, M. Izadi, N. A. C. Sidik, and H. W. Xian, "Forced convection of nanofluids in an extended surfaces channel using lattice Boltzmann method," *International Journal of Heat and Mass Transfer*, vol. 117, pp. 1291–1303, 2018.

[3] H. Heidary and M. J. Kermani, "Heat transfer enhancement in a channel with block(s) effect and utilizing Nano-fluid," *International Journal of Thermal Sciences*, vol. 57, pp. 163–171, 2012.

[4] M. H. Esfe, A. A. A. Arani, A. H. Niroumand, W.-M. Yan, and A. Karimipour, "Mixed convection heat transfer from surface-mounted block heat sources in a horizontal channel with nanofluids," *International Journal of Heat and Mass Transfer*, vol. 89, pp. 783–791, 2015.

[5] A. Akbarinia and A. Behzadmehr, "Numerical study of laminar mixed convection of a nanofluid in horizontal curved tubes," *Applied Thermal Engineering*, vol. 27, no. 8-9, pp. 1327–1337, 2007.

[6] H. F. Oztop and E. Abu-Nada, "Numerical study of natural convection in partially heated rectangular enclosures filled with nanofluids," *International Journal of Heat and Fluid Flow*, vol. 29, no. 5, pp. 1326–1336, 2008.

[7] Y. Huo and Z. Rao, "The numerical investigation of nanofluid based cylinder battery thermal management using lattice Boltzmann method," *International Journal of Heat and Mass Transfer*, vol. 91, pp. 374–384, 2015.

[8] T. Ambreen and M.-H. Kim, "Comparative assessment of numerical models for nanofluids' laminar forced convection in micro and mini channels," *International Journal of Heat and Mass Transfer*, vol. 115, pp. 513–523, 2017.

[9] M. Sheikholeslami, S. A. Shehzad, and Z. Li, "Nanofluid heat transfer intensification in a permeable channel due to magnetic field using lattice Boltzmann method," *Physica B: Condensed Matter*, vol. 542, pp. 51–58, 2018.

[10] I. Khan, K. A. Abro, M. N. Mirbhar, and I. Tlili, "Thermal analysis in Stokes' second problem of nanofluid: Applications in thermal engineering," *Case Studies in Thermal Engineering*, vol. 12, pp. 271–275, 2018.

[11] Y. Xuan and W. Roetzel, "Conceptions for heat transfer correlation of nanofluids," *International Journal of Heat and Mass Transfer*, vol. 43, no. 19, pp. 3701–3707, 2000.

[12] J. C. Maxwell, *A treatise on electricity and magnetism, Vol I-II*, Oxford: Clarendon Press, 1873.

[13] H. C. Brinkman, "The viscosity of concentrated suspensions and solutions," *The Journal of Chemical Physics*, vol. 20, no. 4, pp. 571–571, 1952.

[14] S. Patankar, *Numerical Heat Transfer and Fluid Flow*, CRC press, 1980.

[15] S. Habchi and S. Acharya, "Laminar mixed convection in a partially blocked, vertical channel," *International Journal of Heat and Mass Transfer*, vol. 29, no. 11, pp. 1711–1722, 1986.

[16] G. H. Tang, W. Q. Tao, and Y. L. He, "Simulation of fluid flow and heat transfer in a plane channel using the lattice Boltzmann method," *International Journal of Modern Physics B*, vol. 17, pp. 183–187, 2003.